Experiments in Fluids (2005) 39: 48–55
DOI 10.1007/s00348-005-0966-8

ORIGINALS

O. S. Jensen · J. P. Kunsch · T. Rösgen

Optical density and velocity measurements in cryogenic gas flows

Received: 31 May 2004 / Revised: 1 March 2005 / Accepted: 3 March 2005 / Published online: 11 May 2005

Abstract This paper presents the application of optical measurement techniques in dense-gas flows in a heavy-gas channel to determine planar two-component (2C) velocity profiles and two-dimensional (2D) temperature profiles. The experimental approach is rather new in this area, and represents progress compared with the traditional techniques based on thermocouple measurements. The dense-gas flows are generated by the evaporation of liquid nitrogen. The optical measurement of both the velocity and density profiles is accomplished by the implementation of particle image velocimetry (PIV) and background-oriented schlieren (BOS) systems. Supplemental thermocouple measurements are used as independent calibrations to derive temperatures from the density data measured with the BOS system. The results obtained with both systems are used to quantify the dilution behavior of the propagating cloud through a global entrainment parameter β. Its value agrees well with the results obtained by earlier studies.

1 Introduction

The widespread storage and transport of liquefied gases like propane can result in the accidental release into the environment of dense-gas clouds. Therefore, the spreading and dilution behavior of dense gases is always a major concern in current risk assessment studies. The spreading behavior of gases strongly depends on the density ratio of the gas to the ambient air. Due to the low temperature of the accidentally released clouds, their density is higher than the ambient value and their propagation dynamics depends on gravity. However, with a density sufficiently close to the one of the ambient air, the gas behaves passively, i.e., it moves with the prevailing flow conditions of the surrounding air. The spreading and dilution behavior of these so-called heavy-gas clouds is investigated here with particle image velocimetry (PIV) (Raffel et al. 1998; Scarano 2002; Willert and Gharib 1991). Additionally, measurements are carried out with the background-oriented schlieren (BOS) method (Dalziel et al. 2000; Meier 2002; Richard and Raffel 2001), which are supplemented by separate thermocouple reference measurements for the extraction of 2D temperature data. The purpose of this study is to assess the applicability of the present measurement techniques in cryogenic gas clouds and to support the modeling activities.

O. S. Jensen (✉) · J. P. Kunsch · T. Rösgen
Institute of Fluid Dynamics (IFD), ETH Zurich,
Sonneggstrasse 3, 8092 Zurich, Switzerland
E-mail: olaf.jensen@ifd.mavt.ethz.ch

2 Experimental setup

The main experimental facility for this study is the heavy-gas channel at the Institute of Fluid Dynamics, ETH Zurich, Switzerland (Fig. 1). It was designed to investigate the propagation of dense clouds, i.e., clouds having densities larger than the ambient air. The density of the released clouds can exceed that of the ambient air by a factor of two, down to a factor close to one at the end of the cloud. This higher density causes the propagation along the floor of the channel. The current setup is chosen to create cryogenic gas clouds through the evaporation of liquid nitrogen under different conditions. The channel has a length of 12 m, is 1.2 meters wide, and has a height of 1 m. It consists of three distinct sections. The first section is the release chamber. Here, the liquid nitrogen is evaporated under controlled conditions to produce clouds with varying properties. The second section is, essentially, a horizontal surface. This section can be used to investigate the ''undisturbed'' propagation of the heavy-gas cloud and is suited for the installation of obstacles like fences or step-like features. The third section is composed of a series of consecutive steps that can be varied in height and length. This

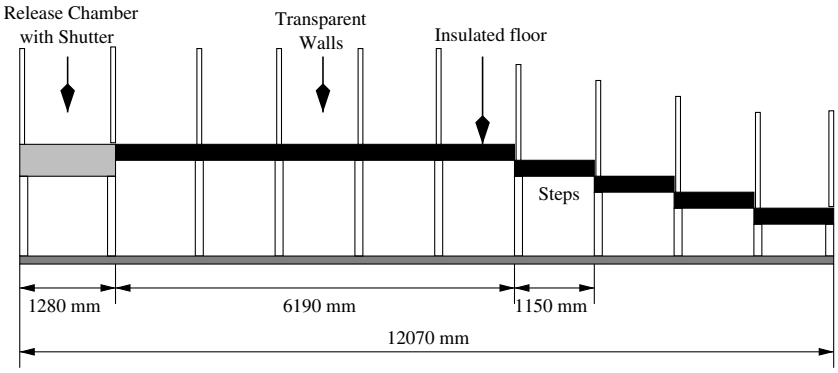

Fig. 1 Schematic view of the heavy-gas channel

section can be compared to idealized topographic features and provides additional acceleration of the flow.

Currently, two different release scenarios can be used to generate cryogenic heavy-gas clouds with variable properties. In the first scenario, the evaporated liquid nitrogen is suddenly released from the release chamber. With the second scenario, it is possible to continuously release a cryogenic gas cloud from a heated Dewar container filled with liquid nitrogen. The additional heating required in this case is provided by immersion heaters.

Only the setup for continuous release will be discussed here. Studies based on the configuration for sudden release are documented e.g., by Jensen et al. (2001) and Jensen (2003).

The continuous-release setup represents a generic configuration, allowing the extraction of well defined parameters of the flow. An electrical heating system is installed in a reservoir of liquid nitrogen large enough to create steady-state measuring conditions for the experiments. By varying the applied power, the amount of evaporated nitrogen can be varied continuously.

The setup for computerized BOS is rather simple, as shown in Fig. 2. For this technique, only few hardware components are necessary. The setup consists mainly of a structured background image (black-dot pattern on transparent background) placed behind the phase object, i.e., the heavy-gas channel, and a camera placed on the opposite side. The camera used here has a 1,000×1,000-pixel resolution. The background image is mounted in front of an electroluminescent sheet, which is used as the light source. This arrangement creates a very uniform illumination of the target pattern. To eliminate effects due to perspective distortions, the camera was placed as far away from the channel as possible. A telelens (focal length up to 200 mm) was used to provide a sufficient resolution of the background image. The two reference temperatures needed for the calculation of the temperature field from the index of refraction in the whole field of view (see Eq. 3) are determined by thermocouple measurements. Probe rakes with nine thermocouples each are placed at the left and right edges of the field of view of the camera. This provides the necessary temperature measurements as close as possible to the imaged area, but without disturbing it. Additionally, the redundant thermocouples can be used for verification purposes.

The experimental setup for the planar two-component (2C) velocity measurements is shown in Fig. 3. It consists of the light-sheet optics, a double-cavity Nd:YAG laser with a pair repetition rate of 15 Hz, and a 10-bit digital camera with 984×1,008-pixel resolution. The camera has a matching acquisition rate of 30 frames per second. The whole optical system is placed on a movable frame. In this way, the system can be positioned anywhere along the channel without changing the relative positions of the optical components. It is possible to generate a light sheet with a thickness of 2 mm and a width of 60 cm at its base while maintaining a high light intensity inside. This allows for a good contrast in the pictures captured with the CCD camera. The field of view normally observed with the camera is about 40-cm high by 40-cm wide. The reason for this fairly large window is the correlation of large structures related to density variations in the ice–particle distribution. These tracer particles are automatically generated during the evaporation process of the liquid nitrogen.

3 Background-oriented schlieren measurements

The BOS technique (Meier 2002; Richard and Raffel 2001), which is similar to "synthetic" schlieren (Dalziel et al. 2000), is used to measure the index of refraction of the cryogenic gas cloud. In the present experiment, this

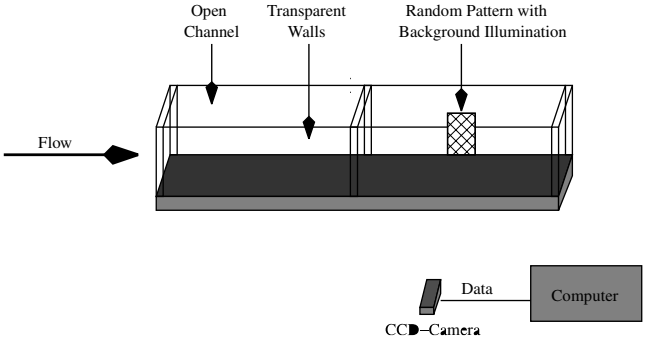

Fig. 2 Schematic view of the setup for background-oriented schlieren (BOS)

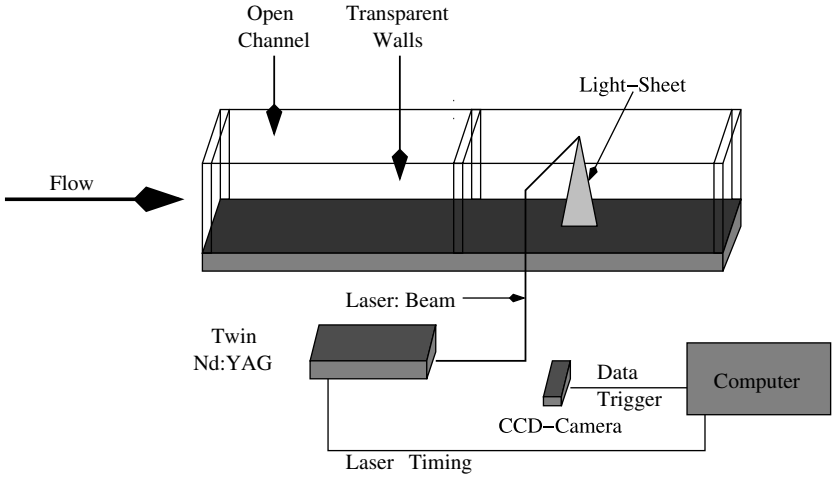

Fig. 3 Schematic view of the setup for particle image velocimetry (PIV)

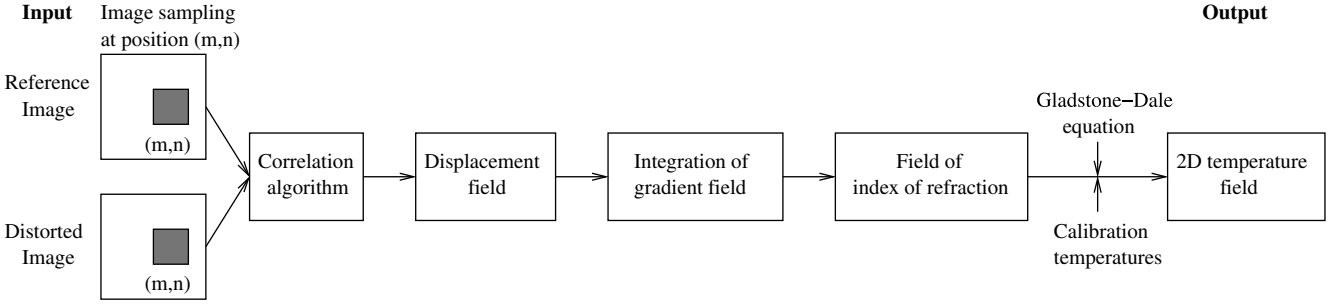

Fig. 4 Flow chart of the temperature calculation with BOS

technique provides the opportunity to deduce the 2D temperature field in a fairly straightforward manner. The technique is based on the distortion of one image, due to density changes, compared to an undistorted reference image. This approach can best be compared with laser speckle density photography, as described by Køpf (1972) and Wernekink and Merzkirch (1987). The processing of the images is shown in Fig. 4. First, an image pair is observed with and without a phase object placed between the background pattern and the camera, as depicted in Fig. 5. The phase object can be, for example, a heat source that changes the temperature and, therefore, the density or a compressible flow pattern. Here, the cold heavy-gas cloud is responsible for the density variations. A typical image pair of one such measurement is shown in Fig. 6. The correlation of both images results in a field of displacement vectors $[\Delta x(x_i, y_i), \Delta y(x_i, y_i)]^T$ in the observed area (Jensen 2003):

$$\begin{aligned} \Delta x(x,y) &= \frac{1}{2} W(W+2B) \frac{1}{n_0} \frac{\partial n}{\partial x} \\ \Delta y(x,y) &= \frac{1}{2} W(W+2B) \frac{1}{n_0} \frac{\partial n}{\partial y} \end{aligned} \quad (1)$$

with the undisturbed index of refraction n_0 and the index of refraction $n(x, y)$ of the phase object. The result is based on the assumption of a 2D index of refraction field with variations only in the x and y directions. This vector field, as shown in Fig. 7, represents the gradient of the index of refraction. Particularly large gradients can be observed in the mixing region between the lower layers of the cryogenic flow and the ambient air. The refractive index $n(x, y)$ can then be calculated with different techniques. One way is to solve the Poisson equation $\Delta n(x, y) = \rho$ in discrete form. Another approach is to directly solve for $n(x, y)$ from the measured field $\nabla n(x, y)$ by using a finite-difference approximation scheme of high order. The latter scheme was used for the results presented here. The calculated index of refraction $n(x, y)$ can be inserted into the Gladstone-Dale equation (Vasil'ev 1971) and, in combination with the equation for perfect gases, gives (for constant pressures):

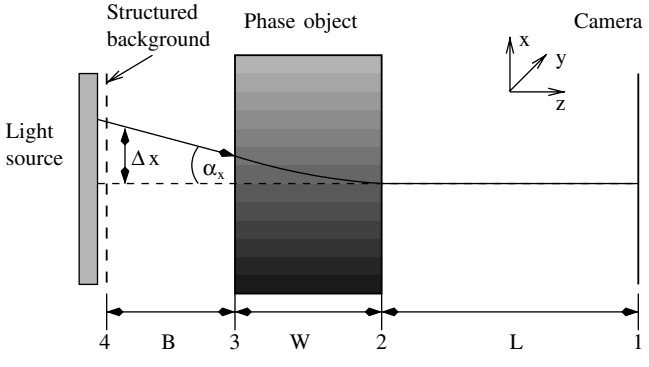

Fig. 5 Sketch of influence of the phase object on rays of light for the y direction. The *dashed line* stands for the case without the phase object

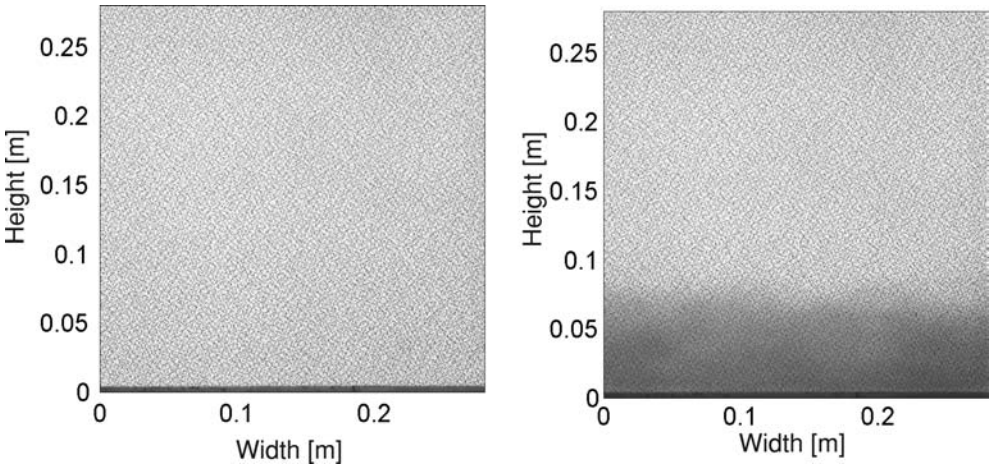

Fig. 6 Typical image pair of a BOS measurement. The *left* picture is the calibration image without the cloud

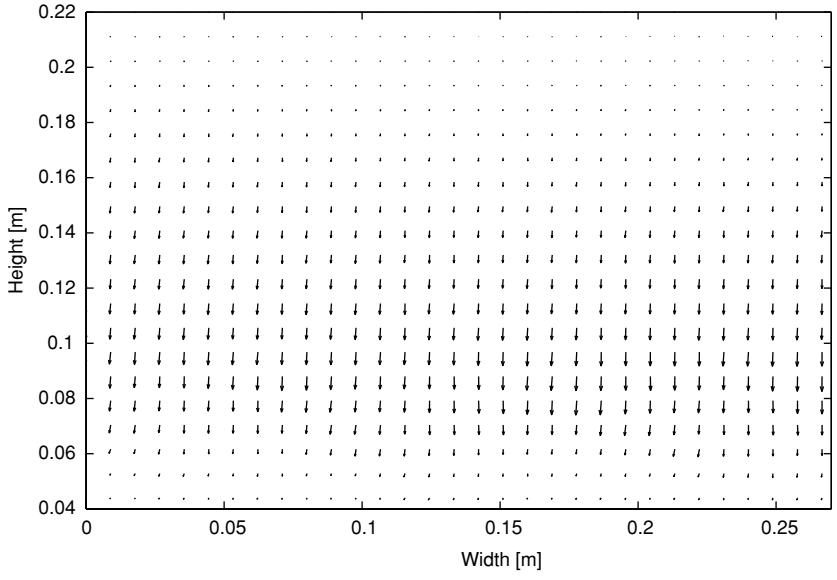

Fig. 7 Displacement of the structured background image due to the phase object

$$n = 1 + \frac{\text{const}}{T} \Rightarrow T = \frac{\text{const}}{n-1} \tag{2}$$

Because the solution for n is determined up to another unknown (calibration) constant, Eq. 2 has to be modified to:

$$T(x,y) = \frac{1}{c_1 \cdot n(x,y) + c_2} \tag{3}$$

with two unknown constants c_1 and c_2, determined by:

$$\begin{aligned} c_1 &= \frac{\frac{1}{T_\text{a}} - \frac{1}{T_\text{W}}}{n_\text{a} - n_\text{W}} \\ c_2 &= \frac{1}{T_\text{W}} - c_1 n_\text{W} \end{aligned} \tag{4}$$

The subscripts a stands for ambient air conditions and W for the conditions close to the wall. The refractive indexes n_a and n_W are taken as the values of the solution $n(x, y)$ at the locations where T_a and T_W are known. The temperature measurements are taken at the same time as the corresponding images.

The measurements presented here are carried out close to the first backward-facing step (Fig. 1) because of the best optical accessibility into the channel at this position. In Fig. 8, the resulting temperatures calibrated with the data from the thermocouple measurements are shown. This temperature field is averaged only over the width of the channel. In fact, all the BOS results presented here are obtained from single image pairs only, because the averaging of several correlation maps only has a very small effect on the quality of the data. The expected increase of the temperature along the x and y directions is clearly visible in Fig. 8, and even more clearly in Fig. 9. Here, the temperature is shown at the left and right edges of Fig. 8, together with the thermocouple measurements. The agreement between both methods is very good. This is more important for the right edge of the image, since both thermocouples used

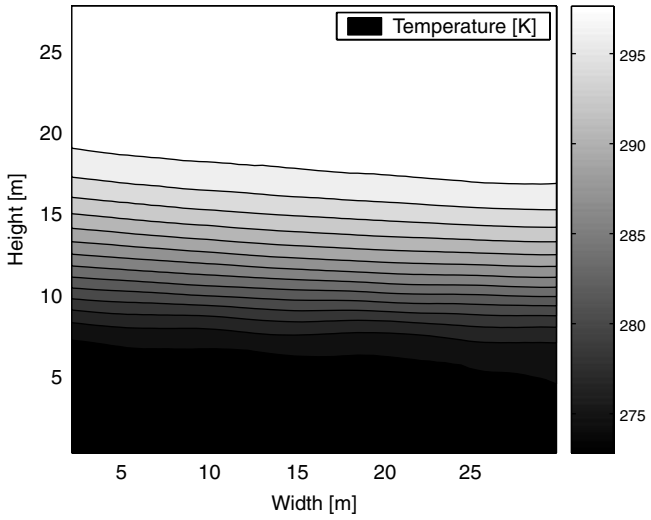

Fig. 8 2D temperature profile in the field of view

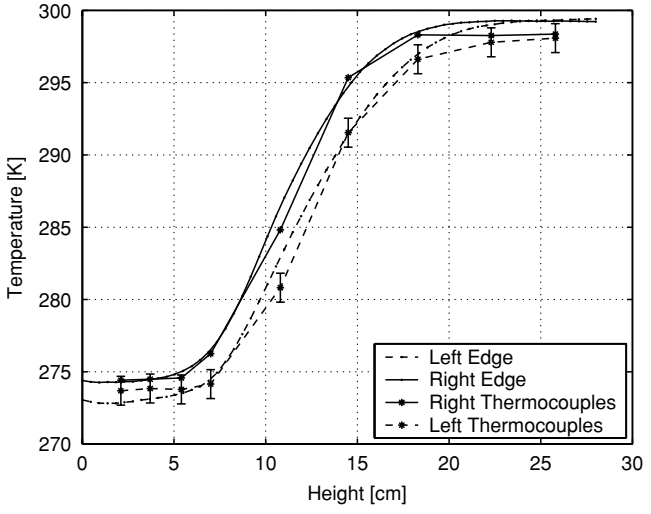

Fig. 9 Temperature distribution over the height at the *left* and *right* edges of Fig. 8, together with thermocouple measurements

for the calibration are located on the left, upstream edge of the image. Therefore, a good agreement between both methods can be expected on the left hand side.

The results presented here are, as stated before, averaged along the line-of-sight. This approach is best used with 2D flows. The correlation of measurements from thermocouples placed 66 cm apart at the same distance downstream from the source of the flow show correlation values of up to 0.8. This justifies the validity of the setup for the measurements presented in this section.

4 Particle image velocimetry measurements

The optical velocity measurements are carried out under the same experimental conditions as the BOS measurements, albeit at different positions due to better optical access into the facility with the setup implemented here. Two types of tracers for the flow visualization are used for the different regions of the flow. The lower layers of the flow are naturally visible due to the ice particles that are automatically generated during the evaporation process of the liquid nitrogen. The upper layers of the flow are visualized by the introduction of talcum powder into the facility where needed. A consequence of the ice particle seeding is the very high number density of the tracers in the flow, so that only the textures visible in the images can be correlated, as shown in Fig. 10.

In Fig. 11, velocity profiles are shown for two positions in the channel. The profiles are computed by averaging three consecutive experimental runs, each generating 150 planar 2C velocity vector maps, i.e., every data point is the average of 450 velocity vector maps. The u velocity (in the x direction) has a nearly constant value above the height of 0.2 m. The height of the boundary between the dense-gas flow and the ambient air can be identified by temperature measurements. According to Fig. 15, this boundary lies approximately at 0.2 m, i.e., where room temperature prevails. The most likely explanation for the non-vanishing u velocity above this boundary is the movement of the talcum-powder seeding itself, and not simply the entrainment motion. Because the seeding is introduced into the flow upstream of the light sheet, its velocity has to be non-zero and, therefore, an additional horizontal momentum is observable in the velocity profiles. The measured velocity profiles depend on the flow conditions of the ambient air and on the way the talcum powder is introduced into the flow. Variations in the velocity

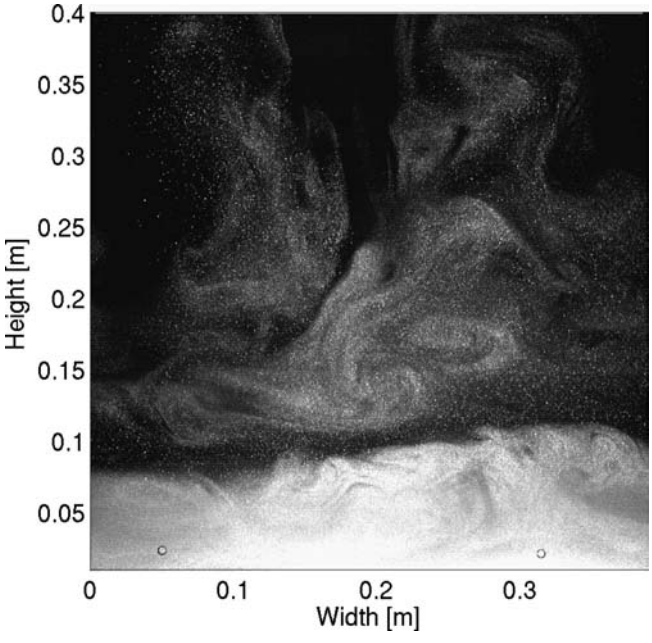

Fig. 10 Snapshot of the flow illuminated with a light sheet

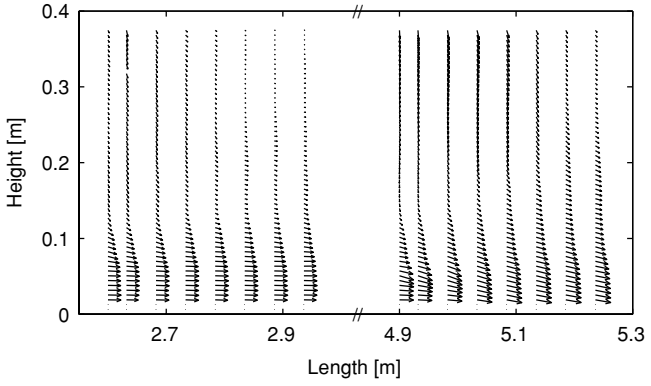

Fig. 11 Velocity profile at two positions in the channel. Further details of the velocity profiles are shown in Fig. 12

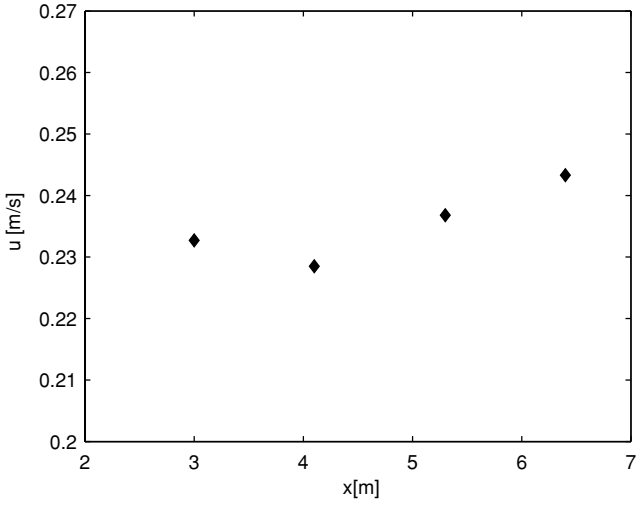

Fig. 13 Velocity as a function of the distance from the release chamber

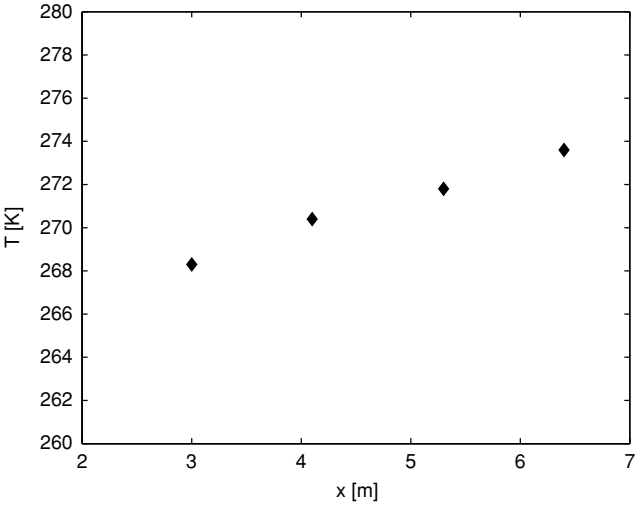

Fig. 14 Temperature measured with thermocouples as a function of the distance from the release chamber

profiles between measurements conducted under similar experimental conditions validate this assumption. The same explanation holds true for the y component of the velocity. The spraying process of the talcum powder is clearly the dominant factor in this case, since a global v velocity (in the y direction) should be very small in the density-driven flow. This assumption is supported by the observation of v velocities being sometimes below and sometimes well within the resolution of the PIV technique in this case. This variation observed under similar experimental conditions can only be caused by the manual introduction of the seeding and, because the talcum powder is introduced into the facility approximately 1 m above the floor of the channel, it should have a negative (downward-pointing) velocity in the chosen frame of reference.

The behavior of the velocity and temperature at different distances from the source is shown in Figs. 13 and 14. These velocities and temperatures cover the lower layer of the dense-gas flow as shown in Fig. 10, which constitutes the more important part of the cloud. Each data point in Figs. 13 and 14 represents one experiment conducted under the same release conditions. The temperature of the cloud increases linearly with growing distance from the source. This can be explained easily by heat transfer from the floor and the entrainment of ambient air into the cloud. The behavior of the velocity as a function of distance from the source is not as obvious as the behavior of the temperature, although a small increase is indicated by the data.

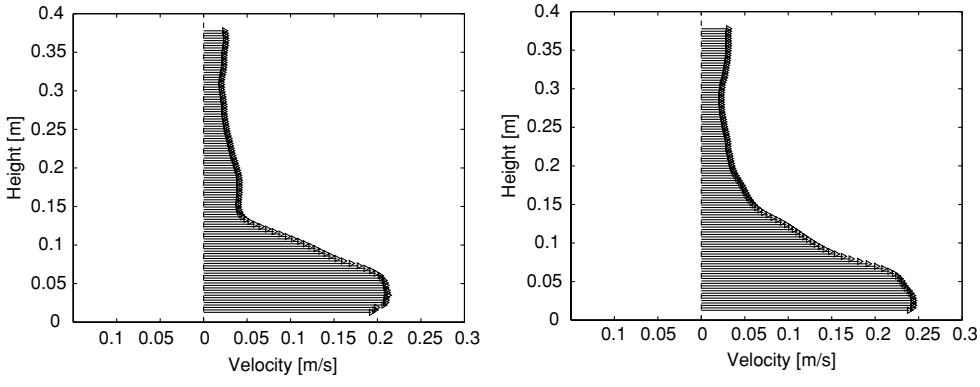

Fig. 12 Averaged velocity profiles at the positions $x_1 = 2.9$ m and $x_2 = 5.25$ m

5 Analysis

An objective of the present experiments was not only to generate a better insight into the basic physics of a dense-gas cloud, but also to extract and interpret the relevant parameters supporting the modeling activities. An important issue is the dilution behavior of a cryogenic dense-gas cloud, which can be described globally by an entrainment parameter.

This parameter can be deduced from a mass and a momentum balance, which are formulated for a generic differential "control volume." This element is defined by a box delimited by an inlet and outlet vertical plane at two locations downstream of the release chamber and the top surface of the cloud propagating between both locations. The inlet and outlet planes are located at $x_1 = 2.9$ m and $x_2 = 5.25$ m, i.e., Fig. 11 represents the control volume. An expression for β is derived in detail in Appendix 1. This expression is evaluated with the experimental information available at both locations x_1 and x_2, as documented in Figs. 14 and 15, to obtain the value $\beta = 0.0026$. This value of the entrainment parameter obtained with the present experimental data, is close to the range $\beta = 0.0028$–0.0037 obtained by Ruff et al. (1988) for their experiments with cryogenic nitrogen. It should be observed that Ruff et al. (1988) used another heavy-gas channel with different release conditions and they evaluated β by means of an energy balance.

The temperature measurements yield almost constant temperatures over the height of the cloud, as documented by the temperature profiles in Fig. 15. The homogeneous temperature distribution is an indication for the intense mixing of the cloud and the dependence of β on heat transfer effects (Kunsch and Fanneløp 1995).

The definition of the entrainment parameter presented so far is simple, and several references making use of β are available for comparison and interpretation (Fanneløp 1994; Ruff et al. 1988). In addition, risk assessment studies, including heavy-gas dispersion in the chain of events, call for simple tools allowing rapid estimates of the propagation and dilution behavior. So, the shallow-layer models for dense-gas clouds require parameters accounting for the complex flow phenomena governing the frontal dynamics or the dilution behavior in a global manner. Hence, even nowadays, there are still good reasons for concentrating the information on the entrainment and dilution behavior of the present experiments in a single parameter. The easy way for extracting the corresponding information, as demonstrated in the present study, may be considered as an example. However, the optical methods presently used are suitable for a more detailed insight into the structure of a dense-gas cloud, e.g., regarding the frontal dynamics or the mixing zone on top of the dense-gas layer.

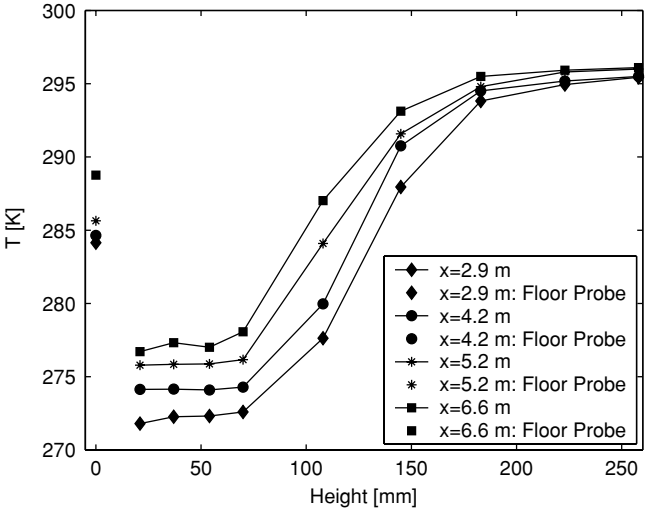

Fig. 15 Temperature profile measured with thermocouples at four positions in the channel

6 Summary and conclusions

The main goal of this study was to investigate the propagation of cryogenic dense-gas clouds with optical methods. Therefore, a particle image velocimetry (PIV) system and a background-oriented schlieren (BOS) system were set up to determine the two important properties; velocity and temperature.

The velocities presented are computed from the flow images obtained using PIV. Due to the properties of the "natural" seeding used, only the textures in the images can be correlated; no individual particles can be identified. As a benefit, this makes it possible to process comparatively large fields of view. Averaged planar two-component (2C) velocity profiles in a viewing area with a size of 40×40 cm could be computed for different positions in the facility.

The temperatures presented in 2D are measured with the BOS system. With a correlation algorithm, the apparent displacement of the image due to variations in the refractive index can be calculated. An in-situ calibration was performed based on discrete calibration temperatures acquired with thermocouples.

The modeling activities could be furthered by using the combined experimental results for velocity and temperature to extract a global parameter that quantifies the dilution of the cryogenic gas cloud during its propagation. An entrainment coefficient β can be derived from a mass balance and a horizontal momentum balance for a differential "control volume" in the heavy-gas channel. The coefficient is close to the values obtained in similar studies conducted by Ruff et al. (1988).

The results presented in this study show the general feasibility to investigate the spreading of cryogenic dense-gas clouds with optical methods. With the applied techniques, the two important distributions of velocity (planar 2C) and temperature (2D) of the propagating clouds could be measured. A PIV system and a BOS system were designed for this purpose. In the context of optical velocity measurements, the simultaneous visual-

ization of the cryogenic gas flow and the ambient air was realized successfully, due to the large field of view employed. The velocimetry system and the schlieren system both allow to derive two-dimensional data. Small-scale structures in both the velocity and temperature, were, however not accessible with the optical methods chosen.

Appendix A

Determination of the entrainment coefficient

The dilution of the cloud is due to the entrainment of ambient air into the cloud, which can be modeled by an entrainment velocity proportional to the horizontal velocity averaged over the height of the heavy-gas layer, i.e.:

$$v_e = \beta u \tag{5}$$

A mass and a momentum balance are formulated for a generic "differential element," defined by a box delimited by an inlet and outlet vertical plane at two locations downstream of the release chamber and the top surface of the cloud propagating between both locations. Both equations are used to deduce β. For modeling purposes, the velocity u and the density ρ, which is actually deduced from the temperature T_a in the cloud, are averaged over the height H of the cloud. The free atmosphere is described by the ambient density ρ_{ae} and the temperature T_{ae}.

The mass balance for the "differential element" reads as follows:

$$\frac{d\dot{m}}{dx} = \frac{d}{dx}(\rho_a u H b) \cong \rho_{ae} v_e b \tag{6}$$

For continuity considerations, the properties (i.e., gas constants and specific heats) of the entrained air and the dense-gas cloud, consisting mostly of nitrogen, are assumed to be the same, and the moisture content of the cloud is neglected. In this case we obtain:

$$\frac{d}{dx}\left(\frac{T_{ae}}{T_a} H u\right) \cong \beta u \tag{7}$$

The horizontal momentum balance for the differential element reads (Rodi 1982) as:

$$\frac{d}{dx}\left[\rho H u^2 - \frac{1}{2} g(\rho_{ae} - \rho_a) H^2\right] = -\tau = -c_f \frac{1}{2} \rho_a u^2 \tag{8}$$

The LHS of Eqs. 7 and 8 are differentiated term by term respectively, and dH/dx is eliminated from both equations. In this case, the entrainment coefficient β can be expressed as a function of the temperature and the velocity gradients in the x direction, which can be obtained experimentally with sufficient approximation, i.e.:

$$\beta = \frac{T_{ae}}{T_a}\left\{H\left[\frac{c_3}{c_1}\frac{1}{u}\frac{du}{dx}\frac{c_2}{c_1}\frac{1}{T_a}\frac{dT_a}{dx}\right] - \frac{1}{c_1}\frac{1}{2} c_f u^2\right\} \tag{9}$$

with $c_1 = u^2 + gH\,(1 - T_a/T_{ae})$, $c_2 = gH\,(T_a/T_{ae} - 0.5)$, and $c_3 = c_1 - 2u^2$. The last term on the RHS in Eq. 9 is related to friction at the ground surface and its value can be up to 30% of the value of the first term. The friction factor c_f is derived from the local friction factor $c'_f = 0.0592(Re_x)^{-1/5}$ for a flat plate, which is averaged over the distance between the inlet and the outlet of the differential control volume. The value $c_f = 0.0064$ obtained is close to the value $c_f = 0.0060$ suggested by (Britter 1987) for dense-gas dispersion.

References

Britter RE (1987) Assessment of the use of cold gas in a windtunnel to investigate the influence of thermal effects on the dispersion of LNG vapour clouds. Engineering Department, Cambridge University, Cambridge, CUED/A-Aero/TR 14

Dalziel SB, Hughes GO, Sutherland BR (2000) Whole-field density measurements by 'synthetic schlieren'. Exp Fluids 28:322–355

Fanneløp TK (1994) Fluid mechanics for industrial safety and environmental protection. Industrial safety series, no 3, Elsevier, Amsterdam, The Netherlands

Jensen O, Kunsch JP, Røsgen T (2001) PIV measurements in a heavy-gas cloud using ice-particle seeding. In: Kobayashi (ed) Proceedings of the 3rd Pacific symposium on flow visualization and image processing 2001 (PSFVIP-3), Maui, Hawaii, March 2001

Jensen OS (2003) Optical density and velocity measurements in cryogenic-gas flows. Switzerland ETH Z Diss. ETH, no. 15259

Køpf U (1972) Application of speckling for measuring the deflection of laser light by phase objects. Opt Comm 5:347–350

Kunsch JP, Fanneløp TK (1995) Unsteady heat-transfer effects on the spreading and dilution of dense cold clouds. J Haz Mat 43:169–193

Meier GEA (2002) Computerized background-oriented schlieren. Exp Fluids 33:181–187

Raffel M, Willert C, Kompenhans J (1998) Particle image velocimetry. Springer, Berlin Heidelberg New York

Richard H, Raffel M (2001) Principle and applications of the background oriented schlieren (BOS) method. Meas Sci Tech 12:1576–1585

Ruff M, Zumsteg F, Fanneløp TK (1988) Water content and energy balance for gas cloud emanating from a cryogenic spill. J Heat Mass Transfer 19:51–68

Scarano F (2002) Iterative image deformation methods in PIV. Meas Sci Tech 13:R1–R19

Vasil'ev LA (1971) Schlieren methods. Israel Program for Scientific Translations, Keter Publishing, New York Jerusalem London

Rodi W (1982) Turbulent buoyant jets and plumes. Pergamon Press, New York

Wernekink U, Merzkirch W (1987) Speckle photography of spatially extended refractive-index fields. Appl Opt 26:31–32

Willert CE, Gharib M (1991) Digital particle image velocimetry. Exp Fluids 10:181–193